International Journal of Impact Engineering 179 (2023) 104653

Contents lists available at ScienceDirect

International Journal of Impact Engineering

journal homepage: www.elsevier.com/locate/ijimpeng

Experimental and numerical analyses of ballistic resistance evaluation of combat helmet using Hybrid III headform

M. Rodriguez-Millan [a,*], I. Rubio [a], F.J. Burpo [b], K.M. Tse [c], A. Olmedo [d], J.A. Loya [e], K.K. Parker [b,f], M.H. Miguélez [a]

[a] Department of Mechanical Engineering, University Carlos III of Madrid, Avda. de la Universidad 30, Leganés, Madrid 28911, Spain
[b] Department of Chemistry and Life Science, United States Military Academy, West Point, NY 10996, United States
[c] Department of Mechanical Engineering and Product Design Engineering, Advanced Technologies Centre, Swinburne University of Technology Level 8, John Street, Hawthorn Campus, Victoria 3122, Australia
[d] FECSA Company Calle de Acacias 3, San Sebastián de los Reyes, Madrid 28703, Spain
[e] Department of Continuum Mechanics and Structural Analysis, University Carlos III of Madrid, Avda. de la Universidad 30, Leganés, Madrid 28911, Spain
[f] Disease Biophysics Group, Wyss Institute for Biologically Inspired Engineering, John A. Paulson School of Engineering and Applied Sciences, Harvard University, 29 Oxford Street, Pierce Hall 318, Cambridge, MA 02138, USA

ARTICLE INFO

Keywords:
Combat helmet
numerical modelling
ballistic impact
traumatic brain injury
back face deformation
dummy Hybrid III

ABSTRACT

Combat helmets are the primary system for protecting the head against ballistic impacts. Generally, combat helmets have been evaluated using a ballistic plasticine head surrogate based on international standards. More realistic human head models have recently been introduced to assess combat helmet performance considering biomechanical requirements. In this work, the Hybrid III dummy head and neck has been introduced to evaluate the performance of the combat helmet against the ballistic impact of live ammunition at different impact locations, considering two different thicknesses of the padding system. A numerical model including a helmet and a Hybrid III head and neck, is developed and validated with our experimental data. The results reveal the influence of the location, where the rear impact leads to the highest risk of brain damage. The effect of pad thickness is closely related to the energy absorbed by the helmet, the backface deformation (BFD), the contact force and the acceleration measured on the head.

1. Introduction

Bullet penetration, falls, are the main causes of military traumatic brain injury (TBI) [1]. Blast-induced shock waves impacting on soldiers propagate, and are transformed into an energy wave inside the brain that disrupts neural networks, cerebrovasculature, and can potentiate traumatic cell death [2]. Based on data recorded by the U.S. Military Health System only, more than 450,000 service members have suffered a brain injury since 2000, with approximately 82% defined as "mild" and 12% as "moderate" and "severe" [3]. Combat helmets offer primary protection against high-energy incident projectiles. The main materials of the helmets are high-performance fiber composites, such as aramid composite, which provides the combat helmet with high penetration resistance due to its excellent mechanical properties and strength-to-weight ratio. As a result, new ballistic helmets have been developed in recent years to improve strength-to-weight ratio [4], such as the U.S. Army IHPS mid-cut helmet (2019) [5], the U.K. VIRTUS helmet (2016) [6] and the Spanish COBAT helmet (2016) [7].

Numerous studies have focused on analyzing the ballistic performance of combat helmets, as reflected in a recent review by Li et al. [4]. From an experimental and numerical approach, combat helmets are rigorously evaluated according to penetration and perforation tests. The U.S. military standard MIL-H-44099A [8] and the European STANAG 2920 [9] focus on the study of combat helmet perforation with fragment simulating projectiles (FSP). The perforation method is performed on both plane specimens of the helmet material and combat helmets [7, 10–13]. Penetration tests follow the U.S. law enforcement standard NIJ-0106.01 [14], measuring the back face deformation after impact on a ballistic plasticine headform [7,11,15–17].

New experimental and numerical methodologies have been developed to further the knowledge of combat helmet performance from a brain injury approach. Experimentally, new techniques have been

* Corresponding author.
E-mail address: mrmillan@ing.uc3m.es (M. Rodriguez-Millan).

https://doi.org/10.1016/j.ijimpeng.2023.104653
Received 22 October 2022; Received in revised form 10 May 2023; Accepted 12 May 2023
Available online 23 May 2023

employed using ballistic load sensing headform (BLSH) to analyze head pressure signals upon 9 mm Full Metal Jacket (FMJ) impacts [17,18]. Another testing method is through human head surrogates of artificial bone filled with ballistic gelatin as a brain simulant to measure skull damage, intracranial pressure, and strains [19]. This method has not been sufficiently analyzed, as proven by the work of Chang et al. [20]. Their study didn't use combat helmets but obtained accelerations and intracranial pressures in the gelatin brain.

From a numerical approach, finite element method (FEM) allows human head models to analyze different brain injury criteria based on forces, stresses, strains, pressures, deformations, or accelerations. Significant efforts have been carried out in this field, and many numerical head models are now found [15,21–24]. An exhaustive review of the current head models is developed in the work of Li et al. [4].

In this study, we performed experimental tests on the composite aramid combat helmet using the surrogate Hybrid III 50th percentile with real ammunition, 9 mm FMJ, under the same conditions of the standard NIJ-0106.01. The surrogate Hybrid III had already been previously used to analyze the ballistic performance of a combat helmet using spherical projectiles [25]. In this work, an experimental and numerical study of the influence of the pad system thickness on the combat helmet is developed. The numerical model of the helmet-dummy head assembly is calibrated and validated with experimental tests. The numerical model allows studying brain injury in a wide range of bullet impact velocities (300-500 m/s), the skull fracture through the contact force between the pad system and the surrogate's head, the energy dissipation between the various parts of the model, and the influence of the correct positioning of the combat helmet on the brain damage.

2. Experimental work

2.1. Experimental procedure and set-up

Experimental tests are conducted on combat helmets using a pneumatic 9 mm caliber gas gun barrel to launch 8 g FMJ, Fig. 1(a) and (b), respectively. Three shot locations (front, sides, and rear of the combat helmet) are conducted at 430 ± 10 m/s in the ballistic laboratory of Fábrica Española de Confecciones S.A. (FECSA).

Photron FastCam SA-Z digital high-speed cameras are used to measure the impact projectile velocity and the movement of the dummy head-helmet set during impact. The selected frame rate (28000 frames per second, fps) and the resolution of 1024 × 744 pixels are for optimal image quality and analysis. The high-speed camera is placed oblique to the impact trajectory, capturing the projectile's entrance and dummy

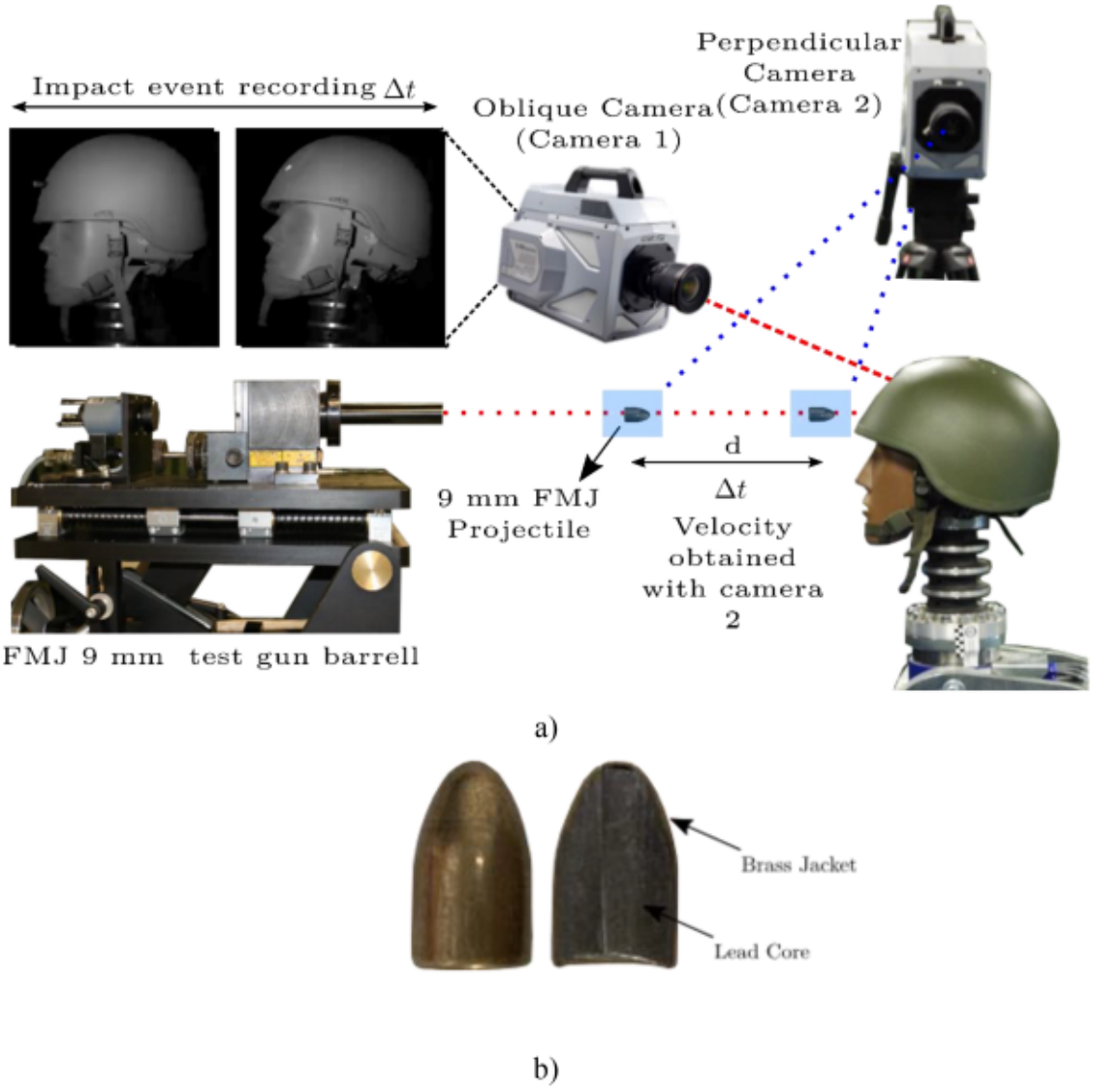

Fig. 1. Experimental set-up. (a) pneumatic cannon, the Hybrid III 50th percentile Anthropomorphic Test Devices (ATD) head and neck and high-speed digital cameras (b) 8 g FMJ.

movement in the same frame, Fig. 1(a). Additionally, a high illumination system (ARRI M18 1800 W) is used to capture the entire impact event with good resolution.

2.1.1. Combat helmet

The aramid combat helmet used in this work, Fig. 2, has a lower weight (8.86 kg/m^2) compared to other models described in the literature, such as Personnel Armor System for Ground Troops (PASGT) or Advanced Combat Helmet (ACH) -9.28 kg/m^2- [25,26]. The pad system consists of six foams with 17 mm (denoted in this work as G-size) and 21 mm (denoted in this work as M-size) thickness to absorb the impact energy, get comfort and guarantee the proper stand-off between the head and the helmet [21]. The pad consists of a two-component foam: a rigid (89.6 kg/m^3) and a softer (86.9 kg/m^3) material. This configuration comprises seven pads (one circular pad at the top of the head, one rectangular pad at the front and one at the back and four oval side pads on each side of the head).

2.1.2. Head surrogates

The head surrogate used for testing is the Hybrid III, 50th percentile, Fig. 1c. It consists of a metallic head form covered by artificial skin and over a surrogate neck. The head is instrumented with three longitudinal acceleration sensors located at its center of mass. The system is perfectly fixed to a heavy weight table fixed to the floor, avoiding any vibration during the test. The weight and diameter of the Hybrid III headform are 4.54 kg and 58 cm, respectively. The numerical modeling section presents a more detailed description of various parts of the complete headform assembly of the Hybrid III dummy.

2.1.3. Ammunition

The projectile 9 mm Luger 124 grain, Full Metal Jacket of Magtech Ammunition, is used to develop this study. The dimensions are specified according to the STANAG 4090 Ed.2 [27]. The bullet has two components: a brass jacket and a lead core (Fig. 1b). This type of ammunition is used for the main security forces and armies in Europe and is specified in several standards NIJ, HOSDB or VPAM [28,29].

2.2. Experimental results

Two helmets have been tested using each type of pad system size, Fig. 2. Two impacts per location and pad system (at the same impact velocity, 430 m/s) are obtained. Peak acceleration and time pulse response are the parameters analyzed. The acceleration time history for the frontal impact is represented in Fig. 3. For the rest of the locations, the curves are similar. Variation of results is found due to the location and impact velocity dispersions (*recorded average impact velocities ranging are 430 ± 10 m/s)*. The maximum peak acceleration at about 0.5 ms, and the duration is approximately 2.5 ms.

The experimental results of the mean peak linear acceleration for all shots are shown in Table 1. The results obtained for the G-size helmet are higher than the M-size helmet in all locations, as expected by having less foam thickness.

According to the NIJ 0106.01 standard, the threshold acceleration to consider brain damage is 400 g. The rear impact for both pad systems is the least safe location considering this threshold. Other studies have also shown that the rear shot is the location with the highest accelerations and force obtained compared to the different impact locations [18,30]. The second most risky location for brain injury is the frontal shot. In this location, the importance of the inner foam is revealed since, for the M-size helmet (the one with the highest thickness), the acceleration is significantly lower than in the G-size helmet, where brain injury would result. In both pad system thicknesses; side shots are not considered likely to result in brain injury.

3. Numerical modeling

This section presents a numerical model of the combat helmet shell, the pad system, the 9mm FMJ projectile and the Hybrid III headform. It

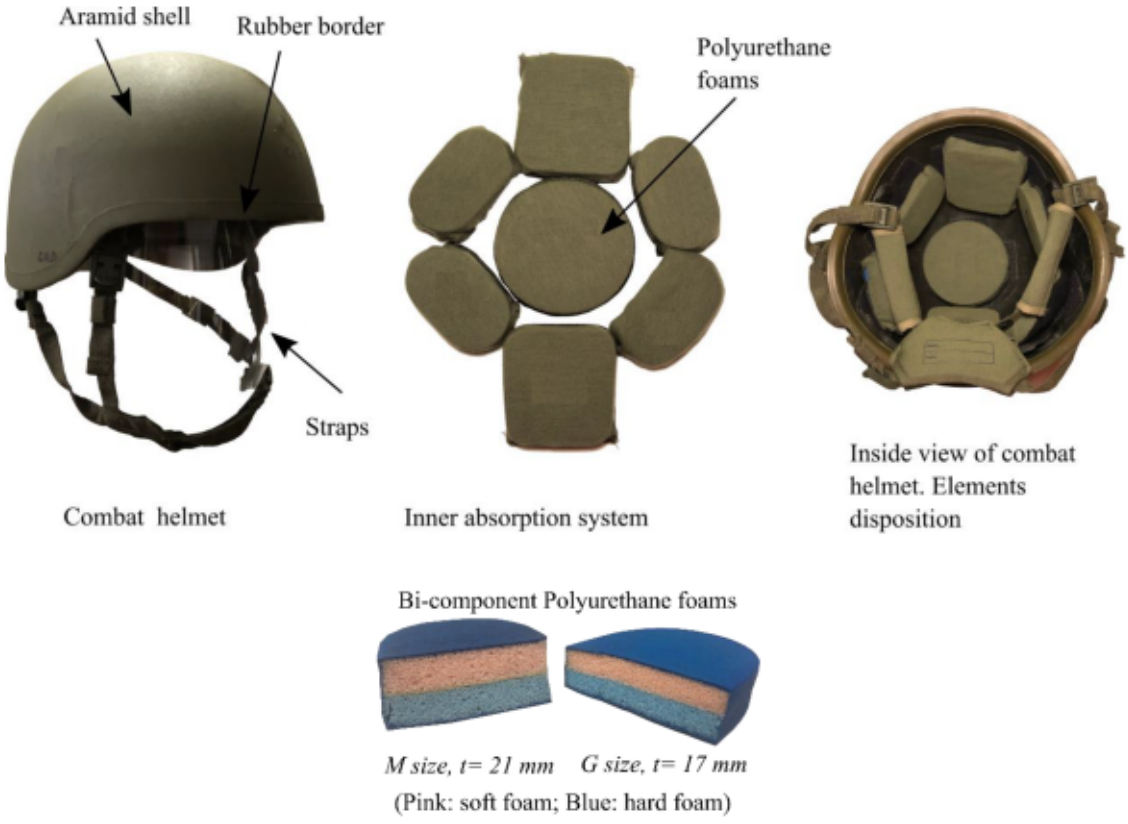

Fig. 2. Combat helmet shell, including inner absorption energy system and straps to hold fast to the head.

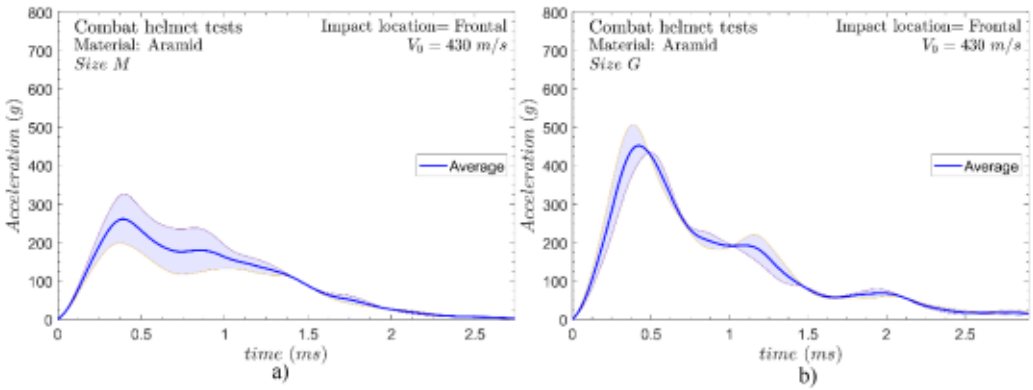

Fig. 3. Resultant linear accelerations temporal history for a frontal shot.

Table 1
Experimental results of peak linear acceleration.

	Mean peak acceleration [g]					
	M-size			G-size		
	Helmet 1	Helmet 2	Mean	Helmet 1	Helmet 2	Mean
Frontal	209.54	336.18	272.9 ± 89.5	518.29	444.50	481.4 ± 52.2
Rear	466.38	599.78	521.3 ± 94.3	534.82	708.10	621.4 ±122.5
Lateral	126.65	85.40	106.0 ± 29.2	178.37	118.73	148.5 ± 42.2

is developed using the commercial finite element code, ABAQUS/Explicit based on a Lagrangian approach, allowing efficient reproduction of the dynamic loading process. The material models, geometries, boundary conditions and mesh are defined below.

3.1. Combat helmet

3.1.1. Combat helmet shell

The combat helmet is modelled using the multi-layer technique presented in earlier works [31,32]. In this study, the layers are grouped in sub-laminate to minimize the computational cost since the cohesive interactions are reduced. Mesh carried out in this numerical model is one element per layer. The number of sub-laminates is used to correctly capture damage due to delamination and shell deformation. The mesh is divided into three different zones (see Fig. 4). The number of elements is different for the numerical models corresponding to three cases studied (frontal, rear and lateral impact). The structure of the seed, however, is the same in all cases.

- Structured zone: this region corresponds to the impact zone of the projectile. The dimensions of this zone are 27 × 27 mm^2 (3 times projectile diameter). It is the most finely meshed area of the helmet model with a characteristic element length of $l_c = 0.75\ mm$.
- Transition zone: this region corresponds to the area between the impact zone of the projectile and the rest of the combat helmet mesh. The dimensions of this zone are 80 × 80 mm^2. A progressive mesh from $l_c = 0.75\ mm$ to $l_c = 4\ mm$ is used.
- Far zone: this region covers the region located sufficiently far from the area directly affected by the impact. It has an element with a characteristic length of 4 mm in zone.

The optimum element size from the impact zone of the projectile was calculated and tested in other work [32] to obtain precision results and a reasonable computational cost.

Aramid composite's behavior is assumed to be elastic up to failure [11,33,34]. All mechanical properties of aramid composite are presented in Table 2, where longitudinal Young's modulus E_1, transverse

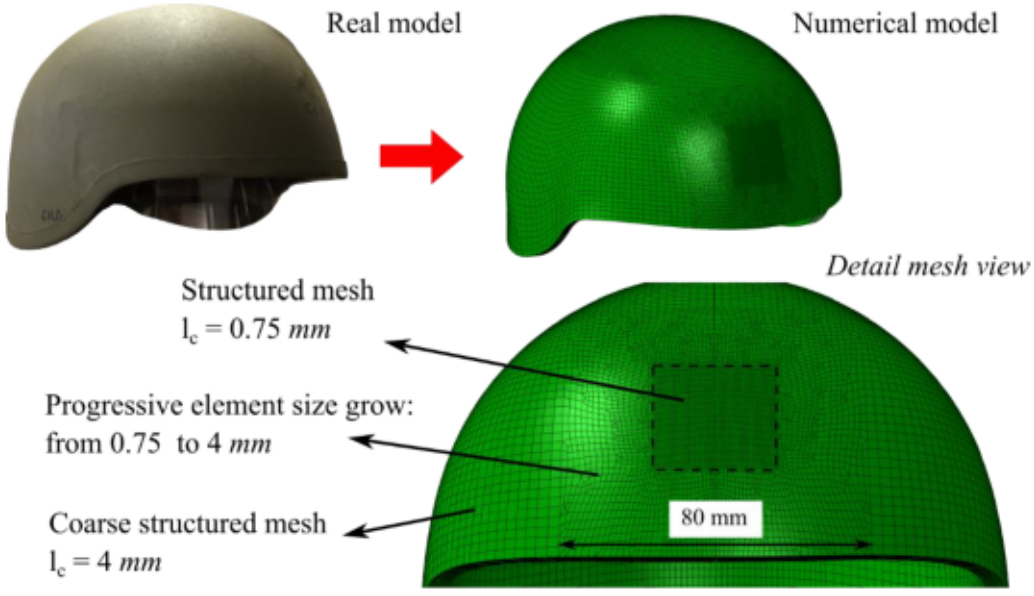

Fig. 4. Helmet mesh used in the numerical simulations.

Table 2
Mechanical properties of aramid composite [41].

E_1 (GPa)	E_2 (GPa)	E_3 (GPa)	G_{12} (GPa)	G_{13} (GPa)	G_{23} (GPa)	$_{12}$ (-)	$_{13}$ (-)	$_{23}$ (-)	(kg/m^3)
22.0	22.0	9.0	0.77	5.34	5.34	0.25	0.33	0.33	1230
S_{1t} (MPa)	S_{1c} (MPa)	S_{2t} (MPa)	S_{2c} (MPa)	S_{3t} (MPa)	S_{3c} (MPa)	S_{12} (MPa)		S_{13} (MPa)	S_{23} (MPa)
800	80	800	80	1200	1200	77		898	898

moduli E_2 and E_3, shear moduli G_{12}, G_{13} and G_{23}, and Poisson s ratios $_{12}$, $_{13}$ and $_{23}$. S_{1T}, S_{1C}, S_{2T}, and S_{2C} are fiber tensile strength, fiber compressive strength in the two directions of the plane 1-2, respectively; S_{12} S_{13} and S_{23} are shear strength. Intra-laminar and inter-laminar failures (delamination) are considered failure models, typically in composite materials.

Intra-laminar failure is predicted using a modification of Hou et al. [35] failure criteria implemented in a VUMAT user subroutine. The failure criterion is based on quadratic form, which helps to account for in-plane and out-of-plane failure modes (Eqs. (1) (3)). Due to the aramid composite presenting a plain wave woven configuration, fiber tensile failure is referred to as the two perpendicular directions on a plane.

In-Plane failure modes (if $_{11}$ $_{22}$ 0

— — — (1)

— — — (2)

Out-of-Plane failure modes

— — — (3)

When one of these criteria is reached (d_i 1), fiber failure is considered. Due to the lower resin content of the composite (9%), the effects of matrix failure (matrix cracking and crushing) are not considered. Like Chang-Chang criteria [36], if the failure occurs, stiffness degradation of composite is simulated by a reduction to zero of stresses involved in the damage mechanism. This reduction of mechanical properties leads to large deformations and element distortion, so it is necessary to include an element erosion criterion based on deformation following the equation proposed by Lopez-Puente et al. [37] to avoid numerical problems.

Cohesive surfaces are used to model the inter-laminar failure of the composite. Cohesive mechanical behavior used in this work is based on traction separation law implemented in Abaqus/CAE [38] in which damage initiation criteria based on quadratic traction and damage evolution law based on energies with linear softening are included. Interface properties used in the numerical model are summarized in Table 3. More details of the constitutive behavior may be consulted in other works [24,32,39,40].

3.1.2. Pad system

The pad system has low density and high compressibility foams with a significant velocity-sensitive behavior. The Low-Density Foam model implemented in ABAQUS [38] is used for this purpose. The stress and compression curves for different strain rates required for the constitutive model are obtained from the literature [25]. The mesh of foams is meshed with hexahedral C3D8R elements and an average size of 2 mm.

Table 3
Cohesive properties used in the numerical model [32].

G_n^c (J/mm^2)	G_t^c G_s^c (J/mm^2)	t_n^0 (MPa)	t_t^0 t_s^0(MPa)	
0.24	0.47	34.5	18.0	1

3.2. Ammunition

The numerical model of the 9 mm FMJ projectile is based on the drawings of STANAG 4090 Ed.2 [27]. It considers the two components of the bullet: a copper jacket and a lead core (Fig. 5). Johnson-Cook model with an Equation Of State (EOS) is used to model the mechanical behavior for both materials, Table 4 [42]. The parameters defined in the table are the density of the materials, , the Shear modulus, G, the reference yield stress, A, the material constants B, n and C, the reference strain rate $\dot{\varepsilon}_0$, the thermal sensitivity parameter m, the melting temperature T_m and a reference temperature T_0. The reference sound speed is denoted as C_0; S , is the slope of the Us Up curve and Grüneisen ratio is $_0$.

The interaction between both parts was defined through general contact using a non-penetration model and a penalty friction coefficient of 0.2.

Adaptive meshing techniques with arbitrary Lagrange/Euler elements (ALE) have been included for the complete projectile in order to avoid distortion problems due to the high strain rates achieved.

3.3. Head surrogates

The numerical model of the Hybrid III headform is developed from drawings provided by Humanetics Innovative Solutions (Plymouth, MI, USA). The Hybrid III model consists of two principal parts: the headform assembly and the neck, Fig. 6. Headform corresponds to hyperelastic skin, metal interior skull (made of magnesium, alloy), with its coupling to neck assembly. Inner to the skull, electronic instrumentation to measure 3-axis linear acceleration are positioned on headform mass center. On the other hand, the neck assembly is formed by a set of metal and rubber disks interleaved, providing the neck with flexion and extension movement. Various parts and materials (mechanical properties) of the dummy hybrid III are shown in Table 5. Headform mass and neck assembly is 4.54 and 1.67 kg, respectively.

The real model of head surrogate presents a steel cable along the interior neck that keeps all elements aligned. This cable does not influence dummy s head response against the movement; it only plays the role of not allowing excessive extension/flexion movement. This cable is not considered in the numerical model. For the Hybrid III headform, the polymer skin is assumed to be constantly in contact with the magnesium skull due to the compressive forces exerted by the stretched polymer onto the skull. Numerically both parts are coupled. The base of the Hybrid III neck is encastred.

For the Hybrid III headform, the polymer skin is assumed to be constantly in contact with the magnesium skull due to the compressive forces exerted by the stretched polymer onto the skull. Numerically both parts are coupled. The base of the Hybrid III neck is encastred.

3.4. Numerical model assembly

The foams are prepositioned undeformed to fix the helmet and foam assembly to the headform, Fig. 7. Then, vertical displacement of the headform and helmet, d, until the distance between the helmet and the

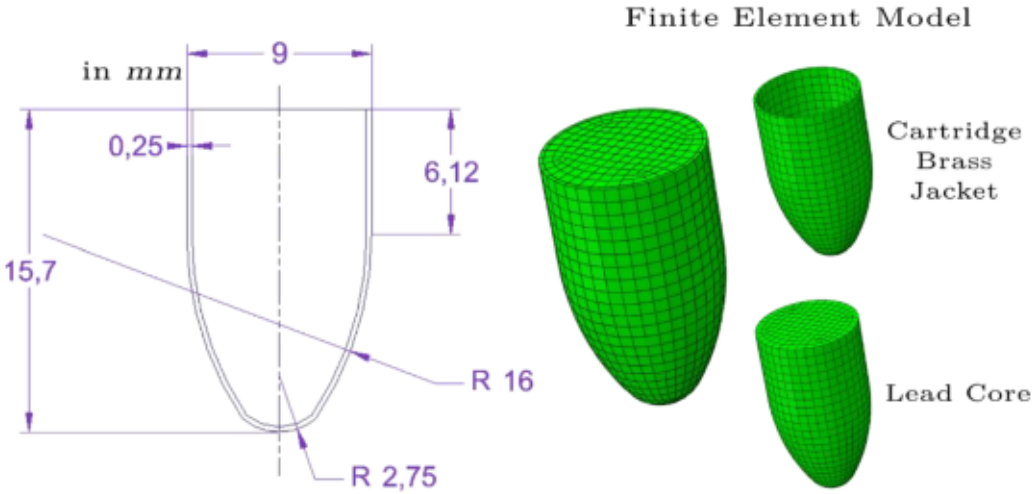

Fig. 5. Experimental and numerical model of Full Metal Jacket (FMJ).

Table 4
Mechanical properties of cartridge brass and lead core[42].

Brass Jacket							
$\rho(kg/m^3)$	$G(GPa)$	$A(MPa)$	$B(MPa)$	$n(-)$	$m(-)$	$\dot{\varepsilon}_0(s^{-1})$	$C(-)$
8520	40000	111	504.69	0.42	1.68	1	0.009
$T_m(K)$	$T_0(K)$	$C_0(m/s)$	S_α	Γ_0			
1189	373	3834	1.429	2			
Lead Core							
$\rho(kg/m^3)$	$G(GPa)$	$A(MPa)$	$B(MPa)$	$n(-)$	$m(-)$	$\dot{\varepsilon}_0(s^{-1})$	$C(-)$
10600	4929	1	55.51	0.098	1	1	0.23
$T_m(K)$	$T_0(K)$	$C_0(m/s)$	S_α	Γ_0			
600	280	2028	1.627	2.253			

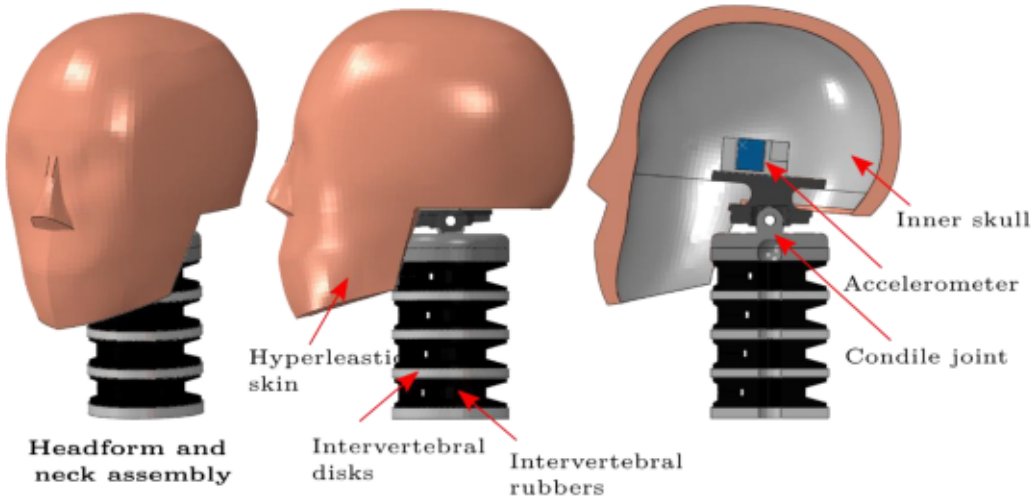

Fig. 6. Numerical model of a 50th percentile Hybrid III dummy.

chin of the head is carried out. The final position of the helmet with respect to headform plays a key role in the acceleration response (keeping constant the impact point respect the helmet boundary). Thus, a study of different distances between helmet and head has been carried out in this work (Section 4.5)

According to the ABAQUS code manual, the contact between the projectiles and the combat helmet is defined with a penalty contact algorithm and hard contact model [38]. The "hard contact" option automatically adjusts the stiffness generated by the "penalty contact algorithm" to minimize penetration without adversely affecting the time increment. Concerning frictional effects, it is assumed a dynamic frictional coefficient μ equal to 0.3 between steel and composite.

The junction between the different non-movable parts of the helmet-dummy headform is performed with the tie constraint. The constraints are all the parts of the dummy (skin-skull, intervertebral metal-rubber disks, head accelerometer mount – inner skull, etc.), the joint of the helmet with the straps and the outer surface of the foams in direct contact with the helmet. In the latter constraint, Velcro is modeled to prevent the foam from sliding due to movement during impacts. The head-neck joint (OC_PIN, Occipital-Condyle Pin) is developed using a

Table 5
Details of the numerical model of the 50th percentile Hybrid III dummy

Part	Material	Constitutive model	Properties	Mass
Skull	Magnesium alloy	Solid Rigid	$I_{xx} = 10750\ kgm^2$ $I_{yy} = 1406\ kgm^2$ $I_{zz} = 12390\ kgm^2$	$m = 2.66\ kg$
Skin	Polymer	a second-order Ogden hyperelastic model [43]	$\mu_1 = 0.318$ $\mu_2 = -0.401$ $\alpha_1 = 1.492$ $\alpha_2 = -3.316$ $D_1 = 10^{-6}$ $D_2 = 10^{-6}$	$m = 1.07\ kg$
Intervertebral disk	Aluminum 6061-T6	Linear elastic	$\rho = 2700\ kg/m^3$ $E = 70\ GPa$ $\nu = 0.3$	$m = 95\ g/disc$
Intervertebral rubber	Rubber	Viscoelastic [25]	$\rho = 2100\ kg/m^3$ $E = 6\ GPa$ $\nu = 0.48$ $G_i(prony) = 0.180647$ $\kappa_i(prony) = 0$ $\tau_i(prony) = 0.012$	$m = 179.4\ g/disc$
Upper & Lower Neck Disk	Aluminum 7076 T6	Linear elastic	$\rho = 2700\ kg/m^3$ $E = 71.1\ GPa$ $\nu = 0.3$	$m = 150\ g/disc$
Condyle joint	Aluminum 7076 T6	Linear elastic	$\rho = 2700\ kg/m^3$ $E = 71.1\ GPa$ $\nu = 0..3$	$m = 170\ g/disc$
Accelerometer & support	Polymer & Al. 6061-T6	Linear elastic	$\rho_{equivalent}\ (polymer) = 3340\ kg/m^3$ $\rho(ac.) = 2700\ kg/m^3$ $E(ac.) = 70\ GPa$ $\nu(ac.) = 0.3$	$m(support) = 60\ g$
Mount	SAE1018 steel	Linear elastic	$\rho = 7800\ kg/m^3$ $E = 200\ GPa$ $\nu = 0.33$	$Mass = 650\ g$

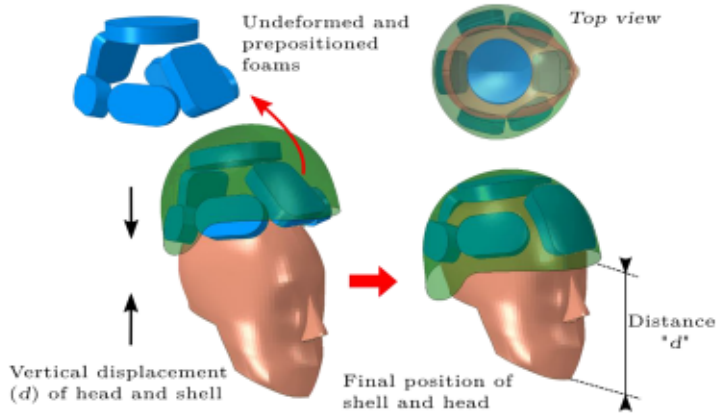

Fig. 7. Numerical model of Hybrid III headform. Methodology for positioning the helmet to the Hybrid III headform and final positioning of the numerical model, "d".

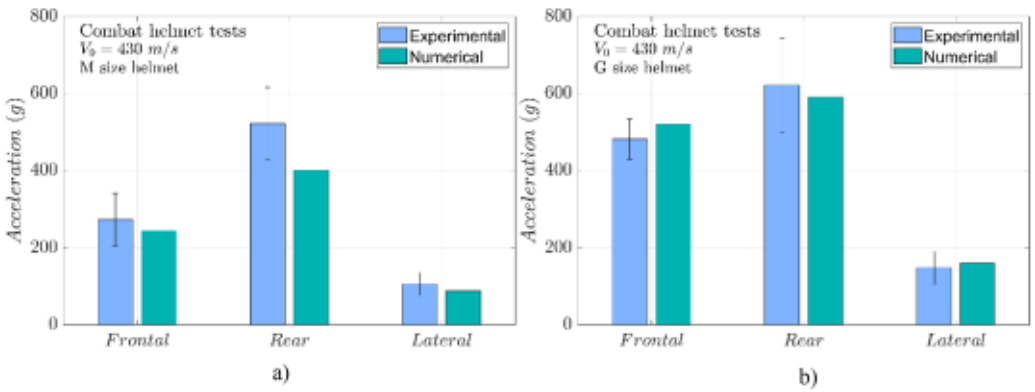

Fig. 8. Comparison of acceleration and impact locations between the impact experiments and simulations for (a) size M and (b) size G at 430 m/s.

kinematic coupling constraint so that the relative motion between both parts can be adjusted by changes in stiffness or displacement restrictions. This work does not consider relative movement between head and neck.

The fabric strap (see Fig. 2) keeps a joint between the helmet and headform and is modeled similarly to actual geometry. The straps support the head and are attached to the helmet by four points. The strap model is modeled as linear elastic with $E = 1$ *GPa and* $\nu = 0.4$ [25].

3.5. F.E.M. validation with experimental data

Numerical simulations are performed under the conditions described in the experimental part, three impact locations at a nominal velocity of 430 m/s. Comparisons between model predictions and experimental measurements of peak linear accelerations in those locations show good agreement, Fig. 8. This figure shows how higher peak linear accelerations are obtained in the case of G size, principally due to the helmet's proximity to the head is lower in the case of thin foam (G-size helmet). Another possible factor is that the impact point location on the helmet is the same regardless of the foam size. In the case of thick foam (M-size helmet), the helmet is positioned higher to the mass center of the dummy, producing less impact force (angular momentum conservation).

An analysis of PBFD (permanent backface deformation) on combat helmets has been used to validate the predictive numerical model. This analysis is carried out using a Hewlett-Packard (H.P.) 3D scan equipment (model H.P. 3D Structured Light Scanner Pro S), obtaining a digital reconstruction of damaged and un-damaged helmets by images. Then, final shapes are exported to GeoMagic ControlX, an inverse engineering software that compares postmortem specimens with undeformed shapes (scanned or CAD models), displaying and quantifying dimensions, defects, etc.

Fig. 9(a) shows the comparison between experimental and numerical results after the impact; the frontal impact example for the M-size helmet is shown. The numerical model obtains PBFD values similar to the experimental observations, 12.98 mm from the simulations compared to 11.46 mm from the experimental test. Fig. 9(b) and (c) show that all PBFD for frontal and rear shots are lower than the threshold value, 25.4 mm, and the PBFD values are lower than the threshold value, 16 mm, for side shots and G-size helmets; however, for M-size, the results are found higher than 16mm, therefore, it may be an injury risk. Therefore, helmet configurations in this work meets the requirements established by the helmet standards, DOT&E protocol [44].

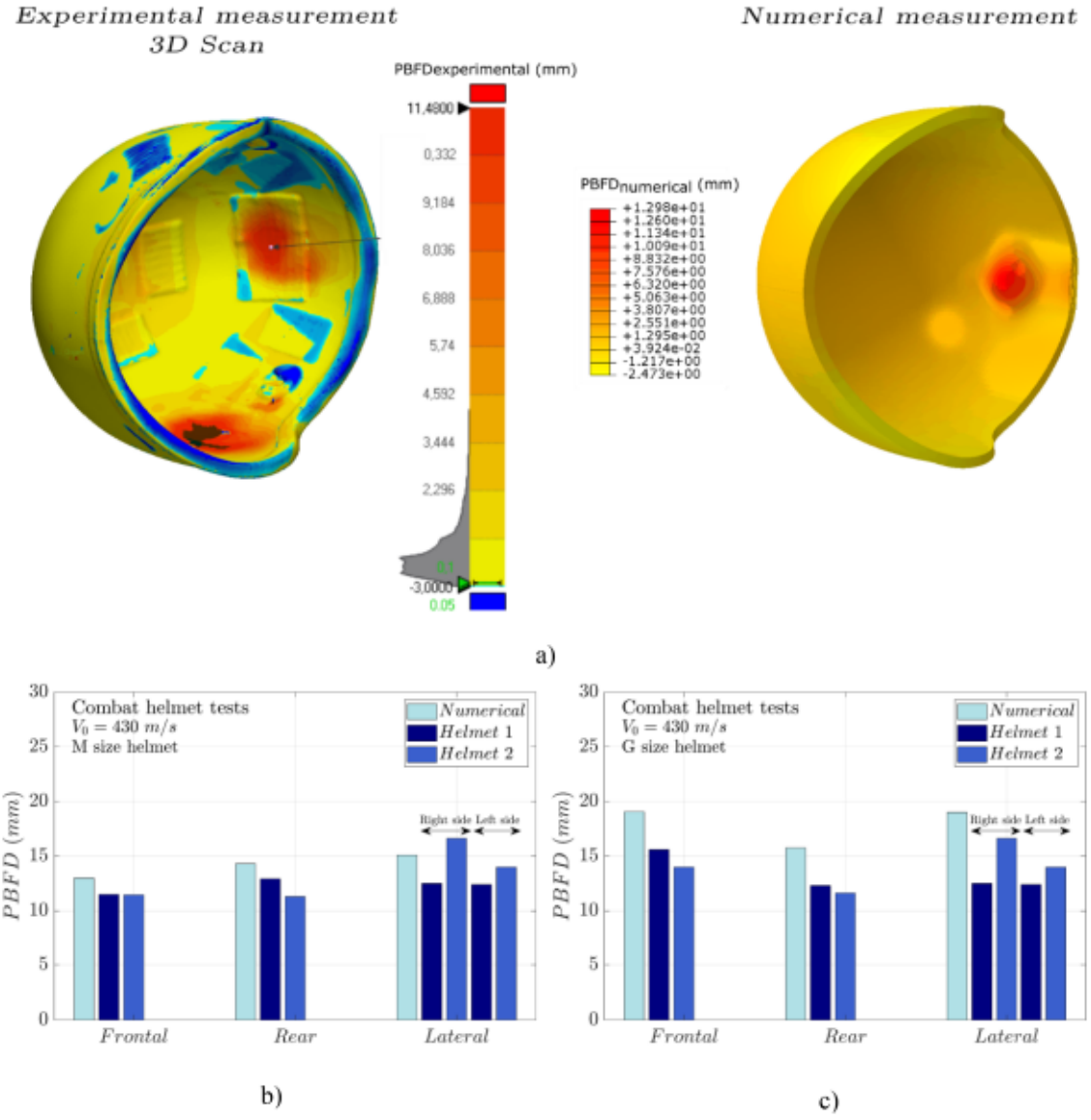

Fig. 9. (a) Experimental and numerical PBFD measurement method. Comparison of PBFD between experimental and numerical results for (b) M-size helmet and (c) G-size helmet. Note that shots are conducted on both sides of the helmets.

Comparing PBFD values reveals an average difference of 25 % between the experimental and numerical results. Therefore, the numerical model faithfully reflects the mechanical behavior of the combat helmet against the ballistic impacts of 9 mm FMJ bullets, and the model validation is considered satisfactory.

4. Results and discussion

The results of the 9 mm FMJ impacts on the Hybrid III human head-mounted aramid helmet are performed in terms of accelerations. TBI may be analyzed from these results with the linear peak acceleration and the Head Injury Criteria (HIC). Furthermore, it can be related to the permanent rear deformation of the postmortem combat helmet.

Numerical simulations allow for analyzing the combat helmet's response with its two sizes of the inner pads at different impact velocities of the 9mm FMJ projectile and obtaining other parameters of interest, such as skull contact forces. Skull forces can be related to the probability of skull fracture.

4.1. Traumatic brain injury (TBI)

The analysis of the brain injury has been performed considering the peak linear accelerations and the duration. This curve was derived by several researchers [45,46] and related peak acceleration to duration and risk of injury. Recently, Hoshizaki et al. [47] updated the Wayne State Tolerance Curve (WSTC) curve through testing of contact sports reported in the literature. The WSTC curve shows that accelerations above the curve lead to injury for a given duration, while no severe damage is derived below it. Many helmet standards are often guided by WSTC data and use linear acceleration thresholds to certify new helmet models [48,49]. The WSTC curve has already been used to analyze combat helmets against ballistic impacts [25].

In the current study, experimental data from tests on size M and G combat helmets at 430 m/s impact velocity are shown for the various locations, Fig. 10. It has been found that only three points are above the WSTC threshold curve. These points are, for G-size helmets, the front and rear locations and the front location for M-size helmets. It should be noted that the case G-size-Frontal is close to the curve. The rest of the cases are far from being considered as having a high probability of brain injury risk. Therefore, the size of the foam and its location are critical for injury prevention.

Another criterion widely used in brain injury analysis for helmet certification is Head Injury Criteria (HIC). This model is developed for the automotive industry. In contrast to the WSTC, the HIC is not limited to the maximum accelerations measured but considers the overall shape of the acceleration curve. The expression to obtain the HIC value is shown in Eq. (4):

$$HIC = \left\{ \left[\frac{1}{t_2 - t_1} \int_{t_1}^{t_2} a(t)dt \right]^{2.5} (t_2 - t_1) \right\}_{max} \quad (4)$$

being t_1 and t_2 the interval time where *HIC* is the maximum value, $a(t)$ is the acceleration measured in g's on the center of gravity. The threshold HIC used in this work was 1000 according to the NHTSA (National Highway Traffic Safety Administration, United Stated) [50] and 2400 proven by the European Standard ECE R22/05 [51]. However, this criterion is controversial for 0 to 5 ms [52].

The severity damage probability can be obtained through the curves developed by Hayes et al. [53] using the Abbreviated Injury Scale (AIS), as shown in Fig. 11.

The HIC values estimated from the accelerations measured in the Hybrid III dummy and the AIS diagnostic metrics [53] are summarized in Table 6. The HIC values that exceed the threshold established by the NHTSA criterion of HIC = 1000 are found in the M-size-Rear, G-size--Frontal and Rear. These results are following the peak liner acceleration (PLA) and WSTC criteria. Regarding the probability of damage, it is found that for a $P(AIS \geq 3)$, it is nearly 100% for the aforementioned cases. For the point of size M and frontal impact, the $P(AIS \geq 3) \approx$ 30%, so it can be considered safe. The TBI associated with *AIS 3* is unconsciousness during 1–6 h and depressed fracture. However, P(AIS=2) =67.8% translates into unconsciousness less than 1 hour and a linear fracture. The brain injury considering the HIC for side-impact cases for both helmet sizes is negligible.

It is again found that foam size is a crucial factor in helmet design for injury prevention.

4.2. Influence impact velocity on brain injury

Numerical simulations allow for analyzing impact velocity's influence on the peak linear acceleration for helmet sizes. The effect found with the numerical results is significant, Fig. 12.

For M-size combat helmets, significant differences between the front and rear locations are found for the wide range of speeds considered. However, for the G-size helmet, the differences are negligible, up to a velocity of 380 m/s. Beyond this velocity, rear impact rapidly increases peak linear acceleration.

The pad system performs better for frontal impacts than rear impacts over the different velocities. It is highlighted that the frontal impact for the M-size helmet is below 400 g, regarded as the acceleration threshold for brain injury by various standards. For the G-size helmet, the critical velocities range 380–390 m/s above which risk of brain injury may appear.

4.3. Influence impact velocity on skull fracture

Behind armor blunt trauma (BABT) is due to contact between the

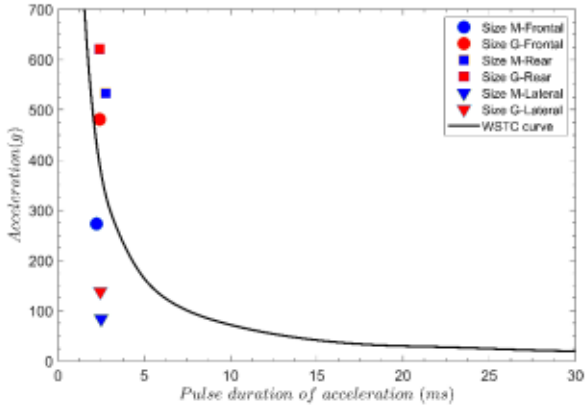

Fig. 10. Comparison of obtained linear acceleration with the threshold tolerance turve of the head injury.

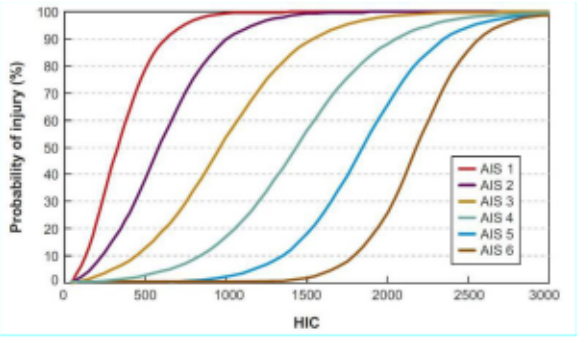

Fig. 11. According to the AIS scale, head injury risk curves are based on the HIC. Data from Hayes et al. [53].

Table 6
HIC and AIS results.

Size	Location	HIC	AIS 1 (%)	AIS 2 (%)	AIS 3 (%)	AIS 4 (%)	AIS 5 (%)	AIS 6 (%)
M	Frontal	745	96.2	67.8	29.1	11.7	0.4	0.0
	Rear	2752	100.0	100.0	100.0	98.5	99.9	99.6
	Lateral	178	18.4	4.5	0.8	0.3	0.0	0.0
G	Frontal	1452	100.0	99.4	86.5	52.7	16.1	1.7
	Rear	2497	100.0	100.0	100.0	96.0	97.7	89.7
	Lateral	276	38.0	11.5	2.5	0.9	0.0	0.0

deformed helmet and the human head, leading to a contact force. The primary trauma involved in BABT is, among others, skull fracture[4]. The contact force between the foam pads and the dummy head model is obtained in this work. Different skull fracture criteria are found in the literature based on the contact forces for blunt impacts. In our study, C. Deck, N. Yoganandan and R. Willinger's skull fracture criterion [54] is used since it is one of the latest criteria developed. They established 4452 N for frontal impact as the thresholds contact force for skull fracture. Fig. 13(a) shows the contact force to impact velocity ratio for the two sizes. Helmet using G-size pad system exceeds the threshold range. However, this limit is reached at 364 m/s and above for the M-size configuration. Fig. 13(b) shows the injury probability with contact force.

Deck, Yoganandan & Willinger's criteria [54] may be arguably applied in analyzing combat helmet ballistic performance. Rafaels et al. [55] revealed that skull fractures are expected to occur for 20-year-old males at projectile velocities greater than 500 m/s using a polyethene combat helmet (30% lighter than an aramid combat helmet, in general). Palomar et al. [21] performed numerical simulations on an aramid combat helmet and established that crack initiation in the skull would occur at 595 m/s and above.

The values obtained in this work are comparable to those obtained in other studies. Li *et al.* [56] found a max contact force of 9.54 kN with a foam pad size of 19 mm on an ACH aramid helmet for an impact of 9 mm FMJ at 370 m/s. Pintar et al. [18] obtained a peak contact force of 6.288 kN for a 9 mm FMJ impact at 360 m/s. The numerical model developed in this study obtained a peak contact force of 4.2 kN for 358 m/s.

Therefore, the influence of the contact force on the prediction of skull fracture for ballistic tests on combat helmets is a challenging topic. There is no experimental data to contrast the results reliably. However, the influence of the foam, and therefore of the stand-off distance, is clear. For a projectile velocity of 430 m/s, the test case with the M-size helmet (stand-off distance=20.5 mm) has a contact force of 6.7 kN, while for the G-size helmet (stand-off distance=14.6 mm), a value of 13.2 kN is obtained, almost double.

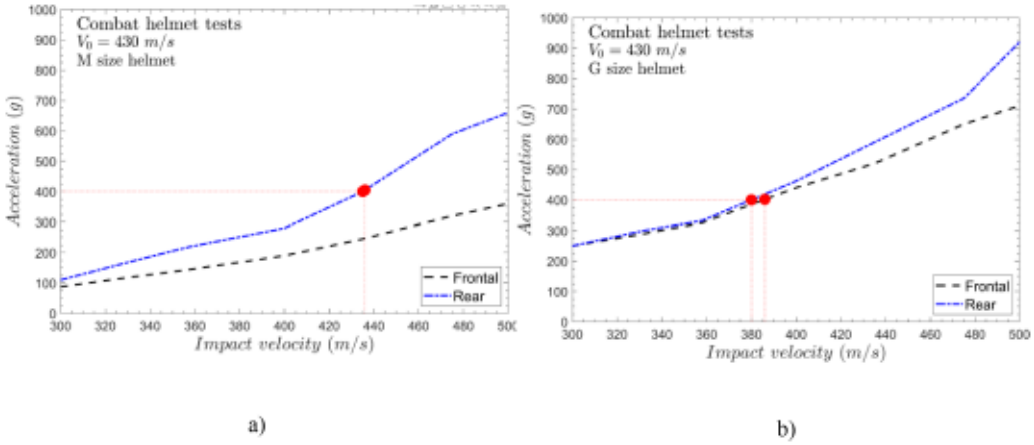

a) b)

Fig. 12. Influence of velocity on the peak linear acceleration for (a) M-size and (b) G-size helmets at 430 m/s.

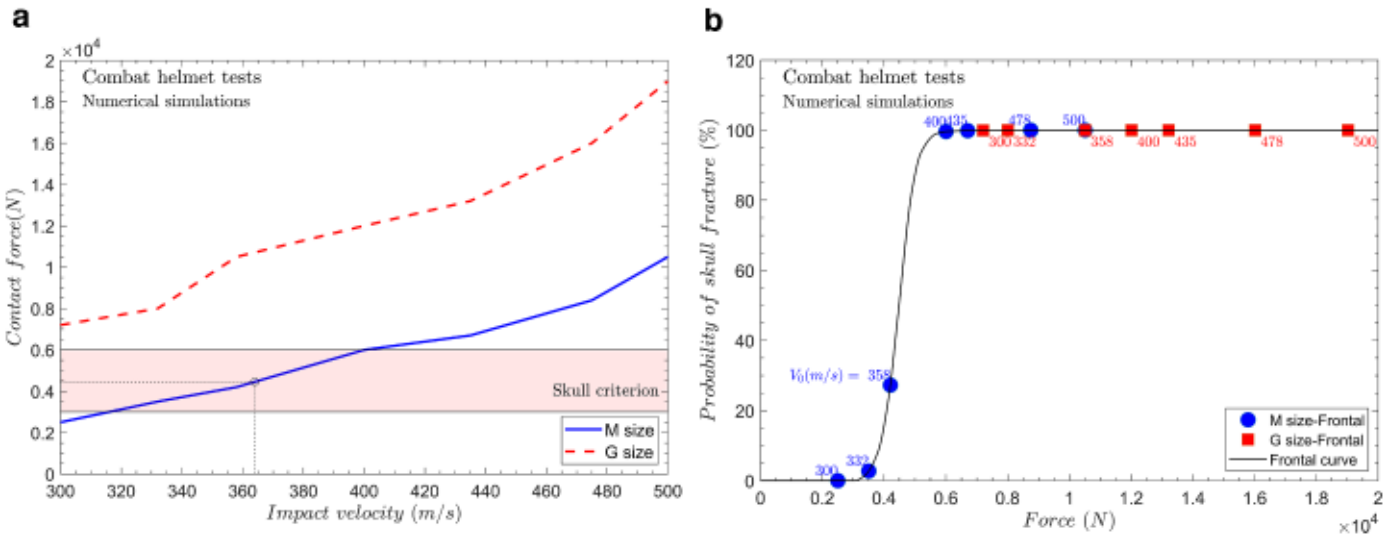

Fig. 13. (a) Relation between contact force and projectile velocity. (b) Probability of skull fracture with contact force.

4.4. Impact energy dissipation

An analysis of the absorption of the initial kinetic energy of the impact in the different parts that make up the complete model is carried out using the numerical model for both pad systems in the frontal shot. The total energy of the system, which remains constant during the whole process, corresponds to the initial kinetic energy of the impact due to the velocity of the 9mm FMJ bullet. The total energy balance of the system follows Eq.5:

$$E_{total} = E^{kin}_{imp} = \sum_i \left(E_i^{kin} + E_i^{intern} + E_i^{visc\ dis}\right) + E_{w.m.}^{frict\ dis} - W_{w.m.}^{ctc\ p} - W_{w.m.}^{const\ p} - W_{w.m.}^{ext} \quad (5)$$

Eq.5 is divided in two: the energies corresponding to the energy absorbed by the different elements E_i (projectile, helmet, pad system, skin simulant, etc.) (+) and the work contributed $W_{w.m.}$ (-), being "*w.m.*" (whole model). E_i^{kin} defines the kinetic energy, E_i^{intern} is the internal energy, and $E_i^{visc\ dis}$ is the volumetric viscous dissipation energy. $E_i^{visc\ dis}$ is energy provided by Abaqus/Explicit to stabilize solutions and has no relation to the energy dissipated by viscoelastic deformation. $E_{w.m.}^{frict\ dis}$ is defined as the energy absorbed by friction effects and is obtained for the whole model (*w.m.*). The work contributed is a combination of $W_{w.m.}^{ctc\ p}$ as work due to contact penalties in contact pairs, $W_{w.m.}^{const\ p}$ defined as constraint penalties and $W_{w.m.}^{ext}$ defined as the work of external forces. The latter two have zero value for the model of this study.

We asked how is the energy balance in the impact of FMJ on combat helmets for different sizes of foam, M and G size, Fig. 14. The helmet, pad system and bullet together absorb 87–91% of the total internal energy because they have large deformations. In both helmet sizes, as expected, the helmet absorbs most of the internal energy through

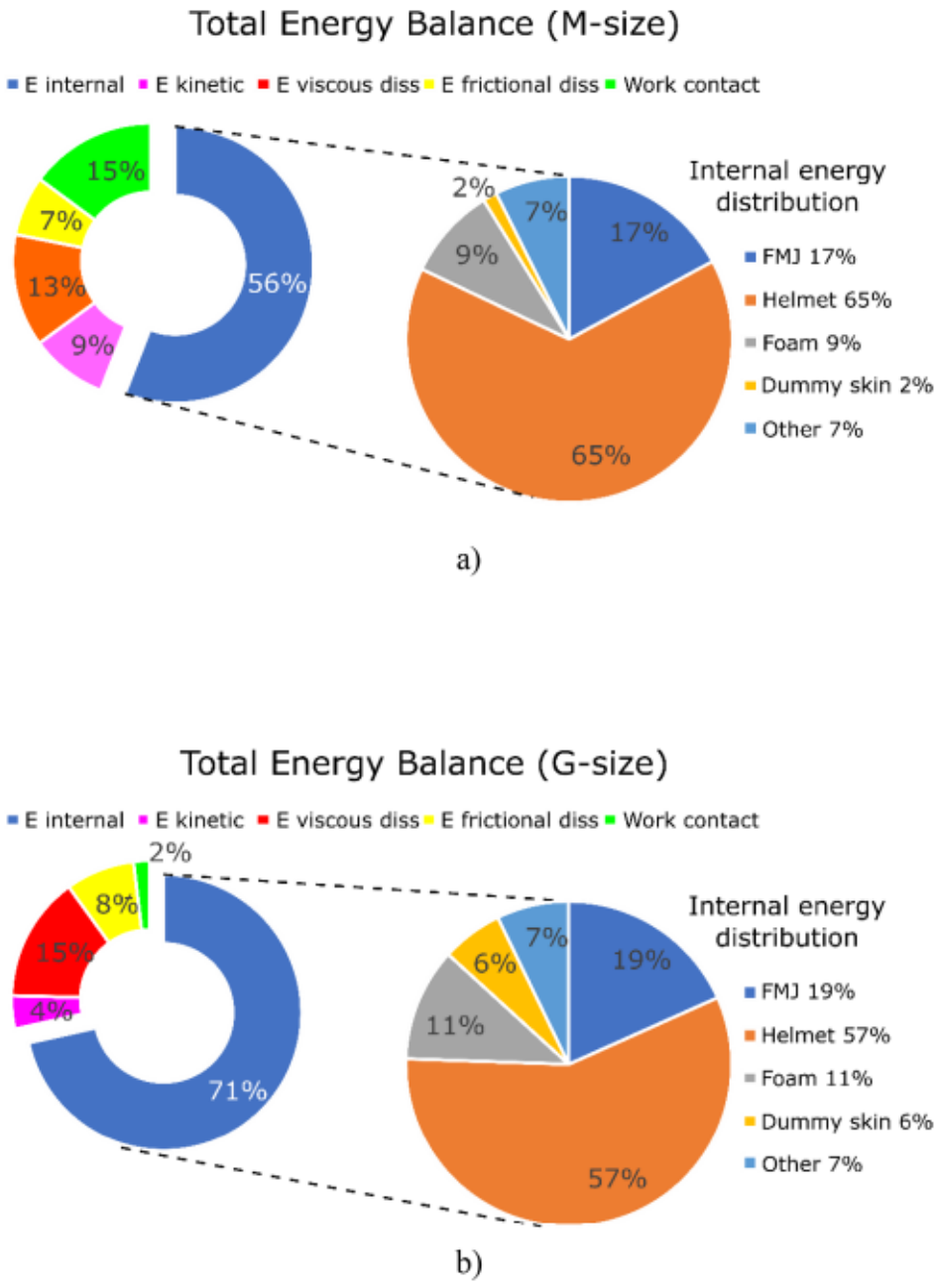

Fig. 14. Energy balance for foam sizes modelled for frontal impact location at 430 m/s impact velocity. (a) M-size helmet (b) G-size helmet.

deformation and failure of the fiber, matrix and delamination, mainly [10,32].

The M-size helmet absorbs higher internal energy (65%) than the G-size helmet (57%). Moreover, the M-size helmet (stand-off distance = 20.5 mm) is deformed (BFD = 19.50 mm) more than the G-size helmet (stand-off distance = 14.6 mm), which is slightly less deformed (BFD = 13.04 mm). The fact that the combat helmets absorb more energy and becomes more deformed leads to the pad system absorbing slightly less energy. Still, combat helmets mitigate the accelerations considerably on the brain by minimizing the brain injury and the contact force on the skull, as observed in Table 7.

Thus, increasing padding thickness improves the helmet's energy absorption, reducing brain and skull injuries. Furthermore, although the recorded values of BFD are lower than the limit values (25.4 mm) established by helmet standards [44], in the case of G size, it is found that it may not adequately prevent brain injury and skull fracture. Therefore, the BFD parameter is not conclusive for a correct evaluation of the performance of the helmets since the analysis of other experimental and numerical parameters such as those proposed in this study may be required.

4.5. Influence helmet height position

The proper positioning of the helmet is essential for user security and depends on the head size, the helmet shell and the pad system. Most studies focusing on the importance of the stand-off distance in minimizing the risk of brain damage have been based on analyzing the thickness of the foam [16,21,56]. The present study also demonstrates that importance. However, it is unfeasible for armies to provide a helmet with a customized padding system for each soldier. Several sizes are available for each helmet model, and different pad thicknesses are used to fit the helmet to the head [21]. Therefore, it is critical to have a helmet that fits correctly on the wearer's head. This section analyzes the correct positioning of the helmet from the wearer's chin to the helmet, denoted by the parameter "d", Fig. 7. Two cases: the user mistakenly wears a helmet of small size (large foam thickness); therefore, the "d" would be large. Or the user wears a helmet with a larger size (small foam thickness), so the "d" would be smaller. For this, the baseline "d" is set at 152 mm, equivalent to a stand-off distance of 20.5 mm. In this study, more numerical simulations are developed for two values of "d", one below, $d_1 = 142\ mm$ (stand-off distance = 17.05 mm) and one above, $d_2 = 162\ mm$ (stand-off distance = 23.10 mm). The simulations are carried out with the 21 mm thick pad system (M-size helmet) for the three impact locations (front, rear and lateral) at a bullet velocity of 430 m/s.

We asked how the accelerations recorded in the dummy Hybrid III vary in the different shooting locations with the distance "d", Fig. 15. The results reveal that the distance "d" is relevant. When the "d" becomes smaller, the acceleration increase is caused since the stand-off distance is smaller, and therefore, less energy is absorbed by the helmet. However, lower accelerations are found for larger values of "d". Does this mean that one should design with a large helmet height position? Undoubtedly not, since the user will have less head area protected. However, the study reveals the importance of positioning the helmet so that the stand-off distance is as considerable as possible, ensuring the most extensive protected area.

5. Conclusions

Traditional combat helmet evaluation methodologies do not necessarily provide good acceleration mitigation and may not provide a higher level of protection against ballistic brain injury. The current method for evaluating the ballistic impact of combat helmets focuses on traumatic brain injury. In this paper, TBI analysis through experimental tests and numerical simulations has been carried out to evaluate the response of a combat helmet subjected to ballistic impacts. The numerical simulation results correlated well with the experimental data in terms of the mechanical behavior of the helmet and accelerations on the head. The method proposed has shown its ability to be used as a design tool.

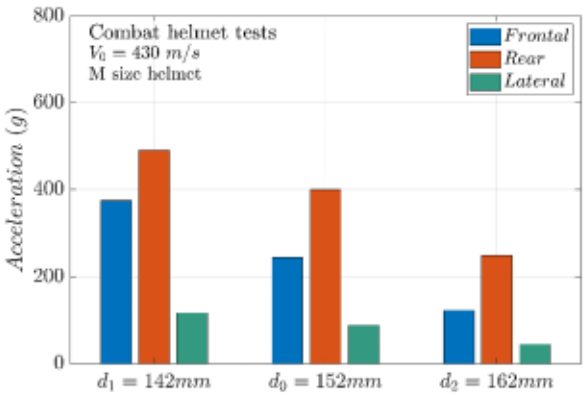

Fig. 15. Comparison between different values of "d" in acceleration for an M-size helmet at 430 m/s bullet velocity.

The results obtained in this paper are synthesized as follows:

- The influence of the foam system thickness was critical to mitigate brain injury according to accelerations. A 1.5-fold increase in thickness led to a 43%, 23% and 39% decrease in terms of accelerations to the thinnest foam system for frontal, rear and side impacts, respectively.
- The shot location that presented the most significant risk of brain injury is the rear, followed by the front and, finally, the sides.
- Contact force is not sufficiently studied to assess skull trauma in ballistic impact combat helmets. Future studies should address the correlation between contact force, skull fracture and bullet velocity.
- The energy balance revealed that most kinetic energy is transferred to the combat helmet. In this study, the energy absorbed by the combat helmet was related to the rear deformation and the stand-off distance. A greater stand-off distance has led to the fact that the helmet can deform more, i.e., more internal energy is absorbed by the helmet and, therefore, less minimization of brain injury and skull trauma were found.
- The position of the helmet height for the chin was intricately linked to the results obtained with the stand-off distance. Increasing the height of the helmet position has involved a greater stand-off distance and, therefore, lower accelerations were found. However, the height should not be abused because it may cause more of the head's face visible.

Declaration of Competing Interest

The authors declare that they have no known competing financial interests or personal relationships that could have appeared to influence the work reported in this paper.

Table 7
Evaluated parameters for frontal impact at 430 m/s.

	Foam thickness (mm)	Stand-off distance (mm)	BFD (mm)	$F_{contact}$ (kN)	Internal energy absorbed by helmet (%)	PLA (g)
M size	21	20.5	19.50	6.7	65	272.9
G size	14	14.6	13.04	13.2	57	481

The authors declare the following financial interests/personal relationships which may be considered as potential competing interests:

Data availability

Data will be made available on request.

Acknowledgments

The authors acknowledge the Ministry of Economy and Competitiveness of Spain and FEDER program under Project RTC-2015-3887-8 and Project DPI2017-88166-R for the financial support of the work. M Rodriguez-Millan acknowledges the Spanish Ministry of Universities, National Program for the Promotion of Talent and its Employability in R&D&I, National Mobility Subprogram of the National Plan for Scientific and Technical Research and Innovation 2021-2023, for the professor s mobility program (PRX21/00329).

References

[1] Kong LZ, Zhang RL, Hu SH, Lai JB. Military traumatic brain injury: a challenge straddling neurology and psychiatry. Mil Med Res 2022;9:2. https://doi.org/10.1186/s40779-021-00363-y.
[2] Hemphill MA, Dauth S, Yu CJ, Dabiri BE, Parker KK. Traumatic brain injury and the neuronal microenvironment: A potential role for neuropathological mechanotransduction. Neuron 2015;85:1177 92. https://doi.org/10.1016/j.neuron.2015.02.041.
[3] Traumatic Brain Injury Center of Excellence. 2022. DOD TBI Worldwide Numbers. Health.mil.DoD numbers for traumatic brain injury: worldwide totals 2000-2021 Q4, as of. February 11, 2022. https://health.mil/Military-Health-Topics/Centers-of-Excellence/Traumatic-Brain-Injury-Center-of-Excellence/DOD-TBI-Worldwide-Numbers (accessed July 13, 2022).
[4] Li Y, Fan H, Gao XL. Ballistic helmets: recent advances in materials, protection mechanisms, performance, and head injury mitigation. Compos Part B Eng 2022;238:109890. https://doi.org/10.1016/j.compositesb.2022.109890.
[5] Avon Protection. F70TM ballistic helmet 2019. https://www.avon-protection.com/products/F70.htm.
[6] Carr DJ, Lewis E, Mahoney P. UK military helmet design and test methods. BMJ Mil Heal 2020;166:342 6. https://doi.org/10.1136/jramc-2018-001123.
[7] Rodríguez-Millan M, Ito T, Loya JA, Olmedo A, Migueles MH. Development of numerical model for ballistic resistance evaluation of combat helmet and experimental validation. Mater Des 2016;110:391 403. https://doi.org/10.1016/j.matdes.2016.08.015.
[8] United States Department of Defense. (1986). Military specification. helmet, ground troops and parachutists. MIL-H-44099A. Retrieved from https://wwwn.cdc.gov/PPEInfo/Standards/Info/MILH44099A%281%29Military specification. helmet, ground troops and parachutists. MILH-44099A. 1986.
[9] NATO Standarization Agency. STANAG 2920 PPS (Edition 2) - Ballistic test method for personal armour materials and combat clothing. NATO Standarization Agency; 2003.
[10] Rubio I, Rodríguez-millan M, Marco M, Olmedo A, Loya JA. Ballistic performance of aramid composite combat helmet for protection against small projectiles. Compos Struct 2019;226:111153. https://doi.org/10.1016/j.compstruct.2019.111153.
[11] Tham CY, Tan VBC, Lee HP. Ballistic impact of a KEVLAR® helmet: experiment and simulations. Int J Impact Eng 2008;35:304 18. https://doi.org/10.1016/j.ijimpeng.2007.03.008.
[12] Nguyen LH, Ryan S, Cimpoeru SJ, Mouritz AP, Orifici AC. The efficiency of ultra-high molecular weight polyethylene composite against fragment impact. Exp Mech 2016;56:595 605. https://doi.org/10.1007/s11340-015-0051-z.
[13] Lim JS, Kim JH. Ballistic behavior of Heracron®-based composites: effect of fiber density and fabrication method. Compos Interfaces 2014;21:543 52. https://doi.org/10.1080/15685543.2014.889966.
[14] National Institute of Justice (NIJ) Standard. NIJ Standard - 0106.01. U.S.D.o. Washington, DC, US: Justice; 1981.
[15] Kwong TM, Bin TL, Yang B, Beng V, Tan C, et al. Ballistic Impacts of a Full-Metal Jacketed (FMJ) Bullet on a Validated Finite Element (FE) Model of Helmet-Cushion-Head. The 5th International Conference on. Computational Methods 2014;(ICCM2014),:1 10.
[16] Palta E, Fang H, Weggel DC. Finite element analysis of the advanced combat helmet under various ballistic impacts. Int J Impact Eng 2018;112:125 43. https://doi.org/10.1016/j.ijimpeng.2017.10.010.
[17] Miranda-Vicario A, Bravo PM, Coghe F. Experimental study of the deformation of a ballistic helmet impacted with pistol ammunition. Compos Struct 2018;203:233 41. https://doi.org/10.1016/j.compstruct.2018.07.012.
[18] Pintar FA, Philippens M, Zhang JY, Yoganandan N. Methodology to determine skull bone and brain responses from ballistic helmet-to-head contact loading using experiments and finite element analysis. Med Eng Phys 2013;35:1682 7. https://doi.org/10.1016/j.medengphy.2013.04.015.
[19] Freitas CJ, Mathis JT, Scott N, Bigger RP, MacKiewicz J. Dynamic response due to behind helmet blunt trauma measured with a human head surrogate. Int J Med Sci 2014;11:409 25. https://doi.org/10.7150/ijms.8079.
[20] Chang L, Guo Y, Huang X, Xia Y, Cai Z. Experimental study on the protective performance of bulletproof plate and padding materials under ballistic impact. Mater Des 2021;207:109841. https://doi.org/10.1016/j.matdes.2021.109841.
[21] Palomar M, Lozano-Mínguez E, Rodríguez-Millan M, Migueles MH, Giner E. Relevant factors in the design of composite ballistic helmets. Compos Struct 2018;201:49 61. https://doi.org/10.1016/j.compstruct.2018.05.076.
[22] Rodriguez-Millan M, Tan LB, Tse KM, Lee HP, Migueles MH. Effect of full helmet systems on human head responses under blast loading. Mater Des 2017;117:58 71. https://doi.org/10.1016/j.matdes.2016.12.081.
[23] Valverde-Marcos B, Rubio I, Antona-Makoshi J, Chawla A, Loya JA, Rodríguez-Millan M. Numerical analysis of BOD helmet under blast load events using human head model. Appl Sci 2020;10:8227. https://doi.org/10.3390/app10228227.
[24] Moure-Guardiola C, Rubio I, Antona-Makoshi J, Olmedo A, Loya JA, Rodríguez-Millan M. Evaluation of combat helmet behavior under blunt impact. Appl Sci 2020:1 22. https://doi.org/10.3390/app10238470.
[25] Bin TL, KM T, Lee HP, Tan VBC, Lim SP. Performance of an advanced combat helmet with different interior cushioning systems in ballistic impact: experiments and finite element simulations. Int J Impact Eng 2012;50:99 112. https://doi.org/10.1016/j.ijimpeng.2012.06.003.
[26] Li YQ, Li XG, Gao XL. Modeling of advanced combat helmet under ballistic impact. J Appl Mech Trans ASME 2015;82. https://doi.org/10.1115/1.4031095.
[27] NATO. (2020). NATO - STANAG 4090 technical performance specification providing for the interchangeability of 9 mm x 19 ammunition.
[28] NIJ. Ballistic standard for ballistic helmets. U.S. Department of Justice National Institute of Justice; 1981. Standard -0106.01.
[29] VPAM, Vereinigung der prüfstellen für angriffshemmende materialien und konstruktionen V. (VPAM)test standard "stab and impact resistance , 2011:1 37.
[30] Tse KM, Tan L, Bin YB, Tan VBC, Lee HP. Effect of helmet liner systems and impact directions on severity of head injuries sustained in ballistic impacts: a finite element (FE) study. Med Biol Eng Comput 2017;55:641 62. https://doi.org/10.1007/s11517-016-1536-3.
[31] Rubio I, Rodríguez-Millan M, Marco M, Olmedo A, Loya JA. Ballistic performance of aramid composite combat helmet for protection against small projectiles. Compos Struct 2019;226. https://doi.org/10.1016/j.compstruct.2019.111153.
[32] Rubio Díaz I, Rodríguez-Millan M, Rusinek A, Migueles MH, Loya JA. Energy absorption analysis of aramid composite during blunt projectile impact. Mech Adv Mater Struct 2021;0:1 12. https://doi.org/10.1080/15376494.2021.1963020.
[33] Van Hoof J. Modelling of impact induced delamination in composite materials [Tesis doctoral. Carleton University]. Carleton University Research Virtual Environment; 1999. https://curve.carleton.ca/d2f24806-c432-42ad-aff5-73edaf23a163.
[34] Shim VPW, Guo YB, Tan VBC. Response of woven and laminated high-strength fabric to oblique impact. Int J Impact Eng 2012;48:87 97. https://doi.org/10.1016/j.ijimpeng.2011.06.008.
[35] Hou JP, Petrinic N, Ruiz C, Hallett SR. Prediction of impact damage in composite plates. Compos Sci Technol 2000;60:273 81. https://doi.org/10.1016/S0266-3538(99)00126-8.
[36] Chang FK, Chang KY. Post-failure analysis of bolted composite joints in tension or shear-out mode failure. J Compos Mater 1987;21:809 33. https://doi.org/10.1177/002199838702100903.
[37] Lopes-Puente J, Zaera R, Navarro C. Experimental and numerical analysis of normal and oblique ballistic impacts on thin carbon/epoxy woven laminates. Compos Part A Appl Sci Manuf 2008;39:374 87. https://doi.org/10.1016/j.compositesa.2007.10.004.
[38] Systemes D. Abaqus v6.14 documentation- ABAQUS analysis user s manual. https://www.3ds.com/support/documentation/users-guides/.
[39] Rubio I, Rodríguez-Millan M, Marco M, Olmedo A, Loya JA. Ballistic performance of aramid composite combat helmet for protection against small projectiles. Compos Struct 2019;226:111153. https://doi.org/10.1016/j.compstruct.2019.111153.
[40] Rubio I, Díaz-alvarez A, Bernier R, Rusinek A, Loya JA, Migueles MH, et al. Postmortem analysis using different sensors and technologies on aramid composites samples after ballistic impact. Sensors 2020;20. https://doi.org/10.3390/s20102853 (Switzerland).
[41] Gower HL, Cronin DS, Plumtree A. Ballistic impact response of laminated composite panels. Int J Impact Eng 2008;35:1000 8. https://doi.org/10.1016/j.ijimpeng.2007.07.007.
[42] Manes A, Bresciani LM, Giglio M. Ballistic performance of multi-layered fabric composite plates impacted by different 7.62 mm calibre projectiles. Procedia Eng. 2014;88:208 15. https://doi.org/10.1016/j.proeng.2014.11.146. Elsevier Ltd.
[43] Wood GW, Panzer MB, Bass CR, Myers BS. Viscoelastic properties of hybrid III head skin. SAE Int J Mater Manuf 2010;3. https://doi.org/10.4271/2010-01-0383. 2010-01 0383.
[44] National Research Council. Review of Department of Defense Test Protocols for Combat Helmets. Washington, DC: The National Academies Press; 2014. https://doi.org/10.17226/18621.
[45] Lissner HR, Lebow M, Evans FG. Experimental studies on the relation between acceleration and intracranial pressure changes in man. Surg Gynecol Obstet 1960;111:329 38.
[46] Gurdjian ES, Roberts VL, Thomas LM. Tolerance curves of acceleration and intracranial pressure and protective index in experimental head injury. J Trauma Inj Infect Crit Care 1966;6:600 4. https://doi.org/10.1097/00005373-196609000-00005.

[47] Hoshizaki TB, Post A, Kendall M, Cournoyer J, Rousseau P, Gilchrist MD, et al. The development of a threshold curve for the understanding of concussion in sport. Trauma 2017;19:196 206. https://doi.org/10.1177/1460408616676503 (United Kingdom).
[48] Rowson B, Duma S. A review of head injury metrics used in automotive safety and sports protective equipment. J Biomech Eng 2022;144. https://doi.org/10.1115/1.4054379.
[49] Whyte T, Stuart CA, Mallory A, Ghajari M, Plant DJ, Siegmund GP, et al. A review of impact testing methods for headgear in sports: considerations for improved prevention of head injury through research and standards. J Biomech Eng 2019;141. https://doi.org/10.1115/1.4043140.
[50] Eppinger, R., Sun, E., Bandak, F., Haffner, M., Khaewpong, N., Maltese, M., et al. (1999). Development of Improved Injury Criteria for the Assessment of Advanced Automotive Restraint Systems - II. National Highway Traffic Safety Administration. National Transportation Biomechanics Research Center (NTBRC). Conrad Technologies, Inc. Vehicle Research & Test Center (VRTC). https://www.nhtsa.gov/.
[51] United Nations, U.N.E.C. for E. ECE 22 05, Uniform Provision Concerning the Approval of Protective Helmets and Their Visors for Driver and Passengers of Motor Cycles and Mopeds; (UNECE), U.N.E.C. for E: Geneva, Switzerland, 2002; pp. 1 11.
[52] Alvarez-Caldas C, Quesada A, Roman JLS, Olmeda E. Head injury criterion: the best way to evaluate head damage? Int J Veh Des 2007;45:411 25. https://doi.org/10.1504/IJVD.2007.014913.
[53] Hayes WC, Erickson MS, Power ED. Forensic injury biomechanics. Annu Rev Biomed Eng 2007;9:55 86. https://doi.org/10.1146/annurev.bioeng.9.060906.151946.
[54] Sahoo D, Deck C, Yoganandan N, Willinger R. Development of skull fracture criterion based on real-world head trauma simulations using finite element head model. J Mech Behav Biomed Mater 2016;57:24 41. https://doi.org/10.1016/j.jmbbm.2015.11.014.
[55] Rafaels KA, Cutcliffe HC, Salzar RS, Davis M, Boggess B, Bush B, et al. Injuries of the head from backface deformation of ballistic protective helmets under ballistic impact. J Forensic Sci 2015;60:219 25. https://doi.org/10.1111/1556-4029.12570.
[56] Li XG, Gao XL, Kleiven S. Behind helmet blunt trauma induced by ballistic impact: a computational model. Int J Impact Eng 2016;91:56 67. https://doi.org/10.1016/j.ijimpeng.2015.12.010.